SLOVAK UNIVERSITY OF TECHNOLOGY IN BRATISLAVA
FACULTY OF ELECTRICAL ENGINEERING AND INFORMATION TECHNOLOGY

MSc. Saman Seifpour

Dissertation thesis abstract

TENSOR DECOMPOSITION ANALYSIS OF EEG SIGNALS DURING BCI-ASSISTED STROKE REHABILITATION

Submitted to obtain the academic title of **Philosophiae Doctor, PhD.**

in the doctorate degree study programme:
Measurement Technology

in the field of study:
5.2.54 Measurement Technique

Bratislava, May 2022

Dissertation thesis has been prepared at Institute of Measurement Science
Slovak Academy of Sciences
Dúbravská cesta 9, 841 01 Bratislava

Author: **MSc. Saman Seifpour**
Institute of Measurement Science
Slovak Academy of Sciences
Dúbravská cesta 9, 841 01 Bratislava

Supervisor: **Prof. Ing. Alexander Šatka, CSc.**
Institute of Measurement Science
Slovak Academy of Sciences
Dúbravská cesta 9, 841 01 Bratislava

Reviewers: **Assoc. Prof. RNDr. Mgr. Kozlíková Katarína, PhD.**
Institute of physics, biophysics, informatics and telemedicine
Faculty of Medicine
Comenius University in Bratislava
Sasinkova 2, 813 72 Bratislava
Slovak Republic

Assoc. Prof. Ing. Erik Vavrinský, PhD.
Institute of Electronics and Phototonics
Faculty of Electrical Engineering and Information Technology
Slovak University of Technology in Bratislava
Ilkovičova 3, 812 19 Bratislava
Slovak Republic

Dissertation thesis abstract was sent on: May 5, 2022

Dissertation Thesis Defence will be held on **.....** at .....**h** (am/pm)

at Institute of Measurement Science
Slovak Academy of Sciences
Dúbravská cesta 9, 841 01 Bratislava

Assoc. Prof. RNDr. Viktor Witkovský, CSc.
Director of IMS SAS

Prof. Dr. Ing. Miloš Oravec
Dean of FEI STU

Abstrakt

Náhla cievna mozgová príhoda (mŕtvica) je jednou z najvážnejších príčin ťažkej dlhodobej invalidity. Cieľom rehabilitácie pacientov po prekonaní cievnej mozgovej príhody s postihnutím končatín je vyvolať neurologické zmeny vedúce k samostatnej pohybovej aktivite využitím neuroplasticity mozgu. Technológia roboticky-asistovaného rozhrania mozgu s počítačom (BCI) využívajúca pacientovu predstavu pohybu (MI) a elektroencefalografiu (EEG) sa stáva jedným z nástrojov pre rehabilitáciu po cievnej mozgovej príhode, ktorý poskytuje sľubné klinické výsledky. V tejto dizertačnej práci sme skúmali zmeny neurálnej aktivity motorických oblastí mozgu využitím EEG signálov, ktoré boli vyvolané počas rehabilitačných tréningov pacienta využívajúcich roboticky-asistované MI BCI. Pre hlbšie pochopenie neurálnych mechanizmov, ktoré sú základom funkčnej obnovy motorických funkcií po poškodení mozgu, v prvom kroku hodnotíme predpokladané neuroplastické zmeny v EEG senzomotorických rytmoch pacienta po prekonaní cievnej mozgovej príhody počas dvoch rokov motorického tréningu pomocou roboticky asistovaného MI BCI. Následne skúmame dynamickú moduláciu oscilačných senzomotorických EEG rytmov, keď si pacient so zatvorenými aj otvorenými očami predstavoval ovládanie externého robotického zariadenia pohybom postihnutej ruky. Aby sme využili informačnú hodnotu nameraných vysokorozmerných dát na vyhodnotenie zmien indukovaných v motorickej kôre počas celého zákroku, používame paralelnú faktorovú analýzu (PARAFAC) na identifikáciu špecifických priestorových a spektrálnych charakteristík nameraných EEG signálov. Súbor lateralizovaných úzkopásmových senzomotorických rytmov špecifických pre konkrétneho pacienta identifikujeme analýzou dominantných priestorových a spektrálnych váh PARAFAC v oscilačnej časti spektra EEG signálov. Zistili sme, že MI BCI-asistovanou rehabilitáciou boli vyvolané dlhotrvajúce zmeny v elektrickej aktivite mozgu pacienta. Tieto zmeny súviseli najmä s dlhodobým zvýšením výkonu pomalých (~ 7.5 až ~ 8.75 Hz) a znížením výkonu rýchlejších senzomotorických rytmov, čo naznačuje ich odlišné, ale komplementárne úlohy pri obnove motorických funkcií. Naše výsledky ďalej ukázali, že oscilačná dynamika tých senzomotorických rytmov, ktorých frekvencie sú centrované na 8.0 Hz a 11.5 Hz bola rozdielne modulovaná v závislosti od toho, či mali pacienti počas experimentov oči otvorené alebo zatvorené. Tiež hodnotíme namerané EEG signály dvoch ďalších pacientov po prekonaní cievnej mozgovej príhody, ktorí sa zúčastnili niekoľkých rehabilitačných sedení. Tu ukazujeme, že tenzorová analýza senzorimotorických EEG rytmov je obzvlášť vhodná na detekciu úzkopásmových aktivít motorickej kôry a poskytuje kvantitatívne informácie o osciláciách neurálnych signálov ľudského motorického systému. Výsledky tohto výskumu prispievajvú k lepšiemu pochopeniu neurálnej plasticity indukovanej dlhodobým motorickým tréningom, ako aj k charakterizácii modulačnej dynamiky ovplyvnenej stavom ľudského oka.

Contents

List of abbreviations and symbols

Abbreviations

BCI	Brain-Computer Interface
EC/EO	Eyes Close/Open
EEG	Electroencephalography
ERD/ERS	Event-Related Desynchronization/Synchronization
ERSP	Event-Related Spectral Perturbation
FFT	Fast Fourier Transform
ICA	Independent Component Analysis
IRASA	Irregular Resampling Auto-Spectral Analysis
MI	Motor Imagery
MI BCI	Motor Imagery Brain-Computer Interface
MIEC/MIEO	Motor Imagery with Eyes Close/Open
PARAFAC	Parallel Factor Analysis
PCA	Principal Component Analysis
PSD	Power Spectrum Density
REC/REO	Resting-state recording with Eyes Close/Open
SMR	Sensorimotor Rhythm

Symbols

A1/A2	Reference electrodes
AFz	Ground electrode
$\mathbf{X}$	A three-dimensional tensor
$\mathbf{X}^{\star}$	The centered tensor across the first mode
I	The number of N-second long EEG epochs for tensor construction
J	The number of EEG electrodes for tensor construction
K	The number of selected EEG frequencies for tensor construction
$\boldsymbol{A}$	Factor matrix representing time signatures for PARAFAC model
$\boldsymbol{B}$	Factor matrix representing spatial signatures for PARAFAC model
$\boldsymbol{C}$	Factor matrix representing frequency signatures for PARAFAC model
$\boldsymbol{G}$	The super-diagonal core tensor for PARAFAC
$\boldsymbol{F}$	The number of PARAFAC factors
$\boldsymbol{E}$	The error term of the model

Introduction

Rehabilitative technologies based on brain-computer interface (BCI) show promising clinical results in the functional recovery of post-stroke patients. However, a better understanding of the effects of using BCI on sensorimotor repair mechanisms by measuring and analyzing electrophysiological signals is still needed. EEG based motor imagery BCI (MI BCI) systems have emerged as a cost-effective and non-invasive technique because of their accurate temporal resolution and their feasibility in clinical environments [Buch et al., 2008; Ang et al., 2011; Chaudhary et al., 2016; Monge-Pereira et al., 2017]. The high dimensionality of BCI-EEG data, especially in a longitudinal motor-training paradigm, is a real challenge for the analysis.

Most signal processing frameworks investigating BCI training effects on neural modulations are univariate. It means that each electrode is considered as an independent source of brain activity. However, due to the volume conduction effect [Nunez et al., 2006], multiple sources of neural activity from different brain regions contribute to the signal recorded at each electrode. While, we here hypothesis that due to neuroplasticity characteristic that enables reorganization of neural pathways in the brain [Murphy and Corbett, 2009], specific brain networks can be activated after each MI BCI training session [Ang et al., 2011; Monge-Pereira et al., 2017]. These networks not only have a specific spatial distribution (laterally distributed over the sensorimotor cortex [Toga and Thompson, 2003; Kapreli et al., 2006]) but also have specific spectral signatures differ based on cortical locations [Donoghue et al., 2021], however, other factors such as experimental conditions, recording time (different days), and tasks could not be neglected [Watrous and Buchanan, 2020]. For such highly multidimensional data, standard matrix factorization methods might fail to represent a rich and informative representation of the data [Cichocki et al., 2008]. Therefore, analytical approaches based on tensor decomposition that encompass these additional dimensions or modes to provide a more natural and informative representations of the original multidimensional data structure should take higher priority.

In signal processing, the term *tensor* refers to an N-way or (multidimensional) array characterized by more than two modes. Large-scale vectors (a one-way array) or matrices (a two-way array) can be represented by higher-order tensors and compressed through tensor decomposition methods into a set of unique multiple components with distinct modalities if they follow a low-rank tensor approximation [Cichocki et al., 2015]. The Parallel Factor Analysis (PARAFAC) [Harshman, 1970; Bro et al., 1997] and the Tucker model [Tucker, 1966] are the two most promising methods for an N-order tensor decomposition. These methods are a generalization of the standard two-way matrix factorization methods such as Discrete Fourier transform (DFT) or principal/independent component analysis (PCA/ICA) by imposing some constraints such as orthogonality, non-negativity, or sparsity of hidden factors [Cichocki et al., 2008]. Although some research has examined the applicability of tensor decomposition methods on properly modeling real and simulated EEG data [Cong et al., 2015; Tangwiriyasakul et al., 2019; Rosipal et al., 2022], the use of these approaches in the BCI domain is gradually developing in recent years. [Liu et al., 2014; Rošťáková et al., 2020b,a].

This thesis aims to evaluate the application potential of advanced numerical methods and algorithms for the quantitative analysis of EEG signals by reducing the dimensionality and revealing the main profiles underlying brain network modulations during after-stroke rehabilitation. To this end, we decompose the multi-channel time-varying EEG signals, recorded over a longitudinal course of MI training using a robotic-assisted MI BCI, into temporal (indicating the motor network activation/deactivation in a given time), spatial (indicating the spatial distribution of the brain networks underlying MI), and spectral (indicating the frequency contents of neural oscillations in the motor-related networks) components with distinct modalities to contribute to a deeper understanding of neural modulations in the sensorimotor brain rhythms following rehabilitation.

1 Goals of the dissertation thesis

Two main specific objectives of the thesis are as follow:

- The first objective of this thesis is to measure and evaluate longitudinal neuroplastic changes in the sensorimotor brain rhythms following rehabilitation. Here, we attempt to show how longitudinal motor training using a robotic-assisted MI BCI can induce short- and long-term effects in the brain's electrical activity in the motor cortex. To the best of our knowledge, this is the first study evaluating the longitudinal short-term (day-to-day) and long-term (over the intervention period) changes in cortical brain activation induced by utilizing an external robotic device triggered by MI of the affected hand and the multiway tensor decomposition concept. In particular, this expands on the study of Rosipal et al. [2019] in which the mirror-box therapy effects on modulation of sensorimotor EEG oscillator rhythms were investigated by proposing a tensor-based approach.
- The second objective of this thesis is to investigate the applicability of a novel analytical framework based on tensor decomposition to precisely measure the underlying dynamics reflecting visual information. We hypothesize the proposed method can contribute to a deeper understanding of the neural mechanism of different eyes conditions (EO vs EC) induced by MI BCI. To the best of our knowledge, however, no prior study has investigated the effect of the open or closed eyes conditions on sensorimotor modulations during MI BCI on stroke patients, while only a few previously published studies are limited to healthy subjects. Part of the aim of this thesis is to further expand on the influence of the eyes-closed condition on the motor cortex, particularly during MI, which received only scant attention in the BCI literature.

2 Material and methods

It should be stressed that the raw data used in this study come from the already existing dataset collected at the Institute of Measurement Science of Slovak Academy of Sciences (UM SAV). The experiment's

paradigm for evaluating the thesis' central question is provided in the first part of this chapter. Theoretical and analytical methods for EEG processing measured during each rehabilitation session are next discussed.

2.1 Participants

A 58-year-old post-stroke male subject who had right-hand hemiplegia due to an is chemic stroke that occurred to him 2 years before participating in this study and affected his left frontotemporal to parietal areas was participated in this study. In addition to the main above-mentioned subject (Patient 1), two other stroke patients with right-hand hemiplegia who had participated in a limited number of rehabilitation training sessions including eight and nine motor training sessions respectively. Subject 2 was a 51-year-old male with right-sided mild hemiparesis that entered this study after two months of an ischemic stroke. Subject 3 was a 45-year-old male with right-sided severe hemiparesis that entered this study after 14 months of an ischemic stroke.

2.2 Experimental procedure

During the experiment, participants were seated in a comfortable chair armrest while their left arms were rested and their right arms were fixed to the robotic splint. Each training session started and ended with two minutes of the resting-state block EEG recordings with closed eyes (REC) condition followed by two minutes with opened eyes (REO). The patient fixated his eyes on a small cross on the wall to control eye movement artefacts during the REO condition. The core of each neurorehabilitation session consisted of training with robotic-assisted MI BCI, during which Patient 1 attempted to control the robotic device by MI of his affected hand. The patient was asked to keep his eyes closed (MIEC) and open (MIEO) while performing the MI task resulting in 10 trials for each MI condition (see Figure 1). While, for Subject 2 and Subject 3, three rehabilitation sessions were scheduled, resulting in 24 and 27 rehabilitation sessions conducted in eight and nine training days, respectively. They also performed the MI task when their eyes were closed, resulting in 30 MIEC trials for each session. The stroke patients had two training days per week in average and each training day lasted an hour approximately.

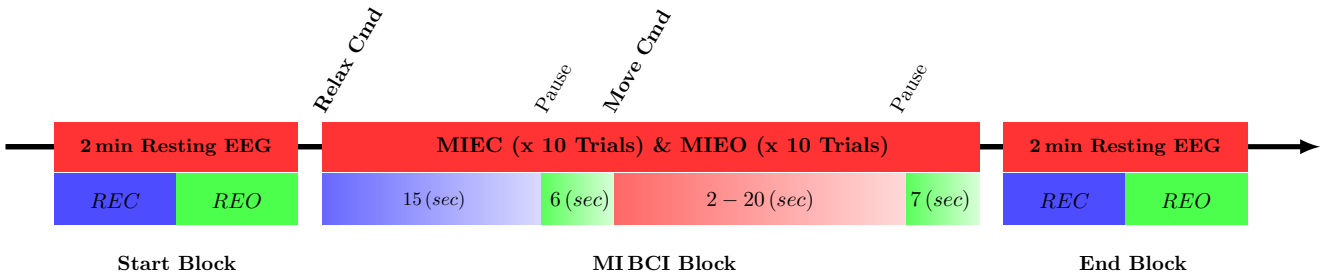

Figure 1: Diagram of each rehabilitation session using robotic-assisted MI BCI. The session started with two minutes resting-state EEG recordings with eyes closed (REC, purple) and eyes open (REO, green) followed by 20 trials of performing MI of the affected hand with eyes-closed (MIEC) and eyes-open (MIEO). A cue sound indicated when the subject had to start the MI (*Move Cmd*) and relax (*Relax Cmd*). These parts separated by implicit transition periods (*Pause*) as buffer zones. The session was ended with the same REC and REO recording blocks as before the MI part.

2.3 EEG data acquisition

EEG signal was continuously recorded by a trained technician using active Ag/AgCl electrodes embedded in an elastic fabric cap (g.GAMMAcap; g.tec medical engineering, Schiedlberg, Austria). The 10 EEG electrodes were placed around the motor cortex according to the extended 10–20 EEG system. Two electrodes covered the left and right primary motor cortex (C3 and C4) with four electrodes around them (FC3/C1/C5/CP3 and FC4/C2/C6/CP4) . One additional electrode was placed at O1 to record posterior Alpha oscillations. The reference and ground electrodes were attached to the left and right ear lobes (A1 and A2) and AFz, respectively (Figure 2, right panel).

2.4 Data preprocessing

At the first step, EEG signals were down-sampled to 128 Hz, and, and an automatic artifact detection with the following criteria was applied. The maximally allowed voltage was set to 50 μV/ms, and the lowest allowed activity in intervals of 100 ms was fixed to 0.5 μV. The maximally allowed difference of voltages in intervals of 20 ms was considered to 50 μV. If any of the first two criteria was met, the interval preceding and following the detected artifact by 150 ms was marked as bad. In the case of the third criterion, this interval was set to 50 ms. Next, a trained technician manually marked periods with undetected artifacts, and removed artifact markers that the software wrongly identified. This step also included the detection and removal of ocular artifacts. The preprocessing step was performed using BrainVision Analyzer 2 software (BVA 2; BrainProducts GmBH, Gilching, Germany).

2.5 Spectral analysis

For the tensor based analysis, the clean multi-channel EEG data including MI training (MIEC & MIEO) as well as task free pre- and post-training resting state data (REC & REO), were segmented into two-second sliding windows with an overlap of 500 ms. But for analyzing the longitudinal changes in oscillatory EEG rhythms, four-second sliding windows with an overlap of 500 ms was considered (only for pre- and post-training resting state data). Then, the irregular-resampling auto-spectral analysis (IRASA) [Wen and Liu, 2016] method was applied to each time window from each single electrode to obtain the raw signal spectrum and its periodic (oscillatory) and aperiodic (non-oscillatory) parts (see Figure 2). In order to truly measure the localized rhythmic activity within a narrow-band frequency range (i.e. oscillatory sources present as narrow-band peaks of power above the aperiodic component), we focused on the oscillatory components only.

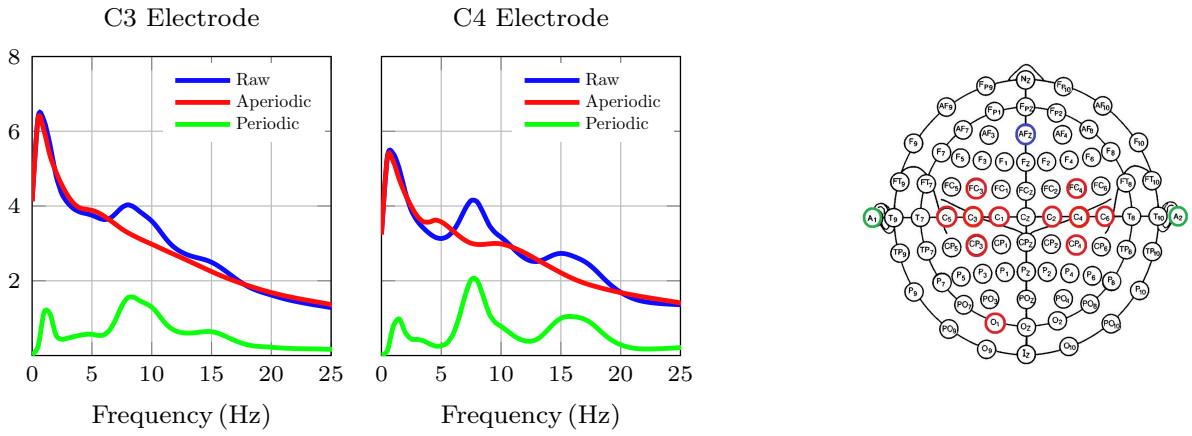

Figure 2: (*left panel*) The irregular-resampling auto-spectral analysis (IRASA) method was employed to extract the periodic (green) activities from the raw power spectra of EEG data (blue) recorded at the left (C3 electrode) and right (C4 electrode) motor cortex during the REC condition after training by robotic-assisted MI BCI. The $1/f$ aperiodic modulations are indicated in red. For visualization purposes, frequencies were restricted to the 0–25 Hz range. (*right panel*) EEG electrodes (red) were placed around the motor cortex. The reference (green) and ground (blue) electrodes are also indicated. The original image configuration comes from Seeck et al. [2017].

2.6 Tensor decomposition

With the aim to identify a set of narrow-band motor-related EEG rhythms, the collected EEG data were modelled by PARAFAC. The logarithmically transformed oscillatory components obtained by IRASA were arranged into a three-dimensional tensor $\mathbf{X} \in \mathbb{R}^{I \times J \times K}$ (*time* $\times$ *electrode* $\times$ *frequency*) where I, J, and K

represent the number of two-seconds long epochs, the number of electrodes ($J = 10$; the O1 electrode was excluded), and the number of selected frequencies ($K = 43$; 4 to 25 Hz with a 0.5 Hz step), respectively. The tensor $\mathbf{X}$ was centered across the first mode:

$$\begin{gathered} \mathbf{X}^{\star}_{ijk} = \mathbf{X}_{ijk} - \frac{1}{I}\sum_{i=1}^{I} \mathbf{X}_{ijk} \\ i = 1, ..., I; \quad j = 1, ..., J; \quad k = 1, ..., K. \end{gathered} \tag{1}$$

The tensor was separately constructed and analyzed for each MIEC and MIEO conditions as well as each training day.

2.6.1 PARAFAC model

A three-way PARAFAC model decomposes the tensor $\mathbf{X} \in \mathbb{R}^{I \times J \times K}$ into three factor matrices $\boldsymbol{A} \in \mathbb{R}^{I \times F}$, $\boldsymbol{B} \in \mathbb{R}^{J \times F}$, $\boldsymbol{C} \in \mathbb{R}^{K \times F}$, and a core tensor $\boldsymbol{G} \in \mathbb{R}^{F \times F \times F}$. The core tensor $\boldsymbol{G}$ is a super-diagonal tensor in which all elements are zero except those on the super-diagonal.

$$\begin{gathered} \mathbf{X}^{\star}_{ijk} = \sum_{f=1}^{F} g_{fff}\, a_{if}\, b_{jf}\, c_{kf} + e_{ijk} \\ i = 1, ..., I; \quad j = 1, ..., J; \quad k = 1, ..., K. \end{gathered} \tag{2}$$

where $\mathbf{X}_{ijk}$ are elements of $\mathbf{X}$, and F is the number of factors that we called *atoms* throughout this paper. The factor matrices are then obtained by minimizing the sum of squared residuals.

$$\sum_{i=1}^{I}\sum_{j=1}^{J}\sum_{k=i}^{K}\left(\mathbf{X}^{\star}_{ijk} - \sum_{f=1}^{F} g_{fff}\, a_{if}\, b_{jf}\, c_{kf}\right)^2 \tag{3}$$

under the constraints:

$$\begin{gathered} \left\|a_f\right\|^2 = \sum_{i=1}^{I} a_{if}^2 = 1, \quad \left\|b_f\right\|^2 = \sum_{j=1}^{J} b_{jf}^2 = 1 \\ \left\|c_f\right\|^2 = \sum_{k=1}^{K} c_{kf}^2 = 1, \quad f = 1, ..., F. \end{gathered} \tag{4}$$

The $\boldsymbol{A}$, $\boldsymbol{B}$, and $\boldsymbol{C}$ factor matrices represent *time signatures* (or *time scores*), *spatial signatures* and *frequency signatures*, respectively (see Figure 3). They have the same number of columns equal to the number of factors ($\boldsymbol{F}$). The tensor $\boldsymbol{E} = (e_{ijk}) \in \mathbb{R}^{I \times J \times K}$ shows the error term of the model. The number of factors in our PARAFAC models varied between six to 20. Then, a cluster analysis was applied to all the extracted atoms from all models Rošťáková et al. [2020b]. Following our previous studies Rosipal et al.

[2019]; Rošťáková et al. [2020b], we imposed the non-negativity constraint on the matrices $\boldsymbol{A}$, $\boldsymbol{B}$, and $\boldsymbol{C}$ to improve the neurophysiological interpretation of the results. Moreover, we considered the unimodality constraint on the matrix $\boldsymbol{C}$ to specifically focus on the localized oscillatory components in the EEG spectrum surrounding a true peak.

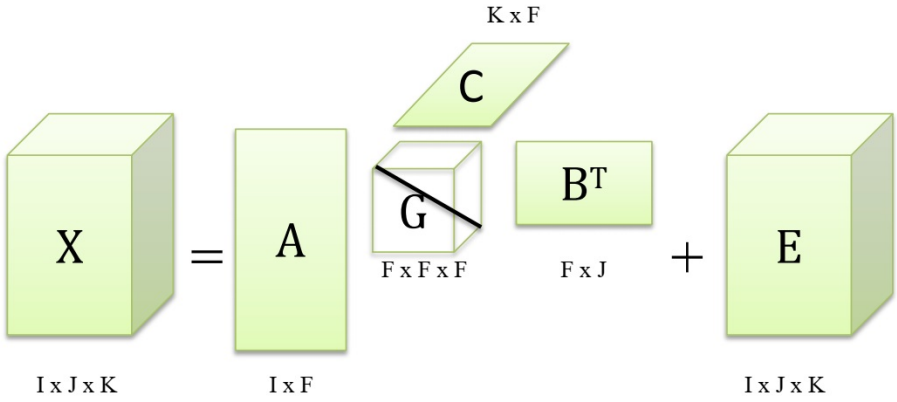

Figure 3: A graphical representation of the PARAFAC model. The original figure comes from [Rošťáková et al., 2020b].

2.7 Time-frequency analysis

To further validate the result obtained by atom-specific time-score averaging and investigate the influence of the MIEC condition on the motor cortex during MI of the affected hand, we computed and visualized event-related changes by calculating time-frequency representations of power. To assess event-related dynamics of the EEG spectrum evoked by the MI onset, we the event-related spectral perturbation (ERSP) analysis. In other words, ERSP allows to visualize event-related changes in the average power spectrum relative to a baseline interval [Grandchamp and Delorme, 2011]. Each data segment was multiplied with a Hanning window and spectral power was estimated using a 256 point sliding Morlet wavelets over a frequency range from 1.5 to 22 Hz with a resolution of 0.25 Hz [Delorme and Makeig, 2004]. The maximum frequency to plot was selected in accordance with the identified narrow-band oscillatory atoms. The minimum number of the Morlet wavelets cycles for the time-frequency analysis was set to 3 that increased linearly with an frequency step size of 0.15 (until the indicated maximum frequency). All power spectra were baseline corrected based on power spectral average in a two-seconds pre-stimulus interval for each frequency band. ERSP was calculated on the C3 and C4 electrodes representing the left and right sensorimotor cortices over the scalp.

3 Detection of subject-specific oscillatory atoms

3.1 Oscillatory rhythms underlying MIEC

The PARAFAC model detected general peak frequencies of oscillatory atoms in the Mu (7.5–8.75 Hz), alpha (9–11 Hz), SMR 1 (11–13 Hz), SMR 2 (13–15 Hz), Beta 1 (15–17 Hz), Beta 2 (17–19 Hz), and Beta 3 (19–21 Hz) frequency ranges. As shown in Figure 4, the PARAFAC model detected seven subject-specific narrow-band oscillatory rhythms. The central peak frequencies of the extracted PARAFAC atoms were at around 8.0, 9.5, 11.5, 14.0, 15.5, 17.5, and 19.5 Hz (forth row) for all subjects. These oscillatory EEG sources are located in the left or right hemisphere, as indicated by spatial signatures (third row) and scalp topography maps (first and second rows). The blue and red curves indicate PARAFAC general atoms for the affected and unaffected cortices, respectively.

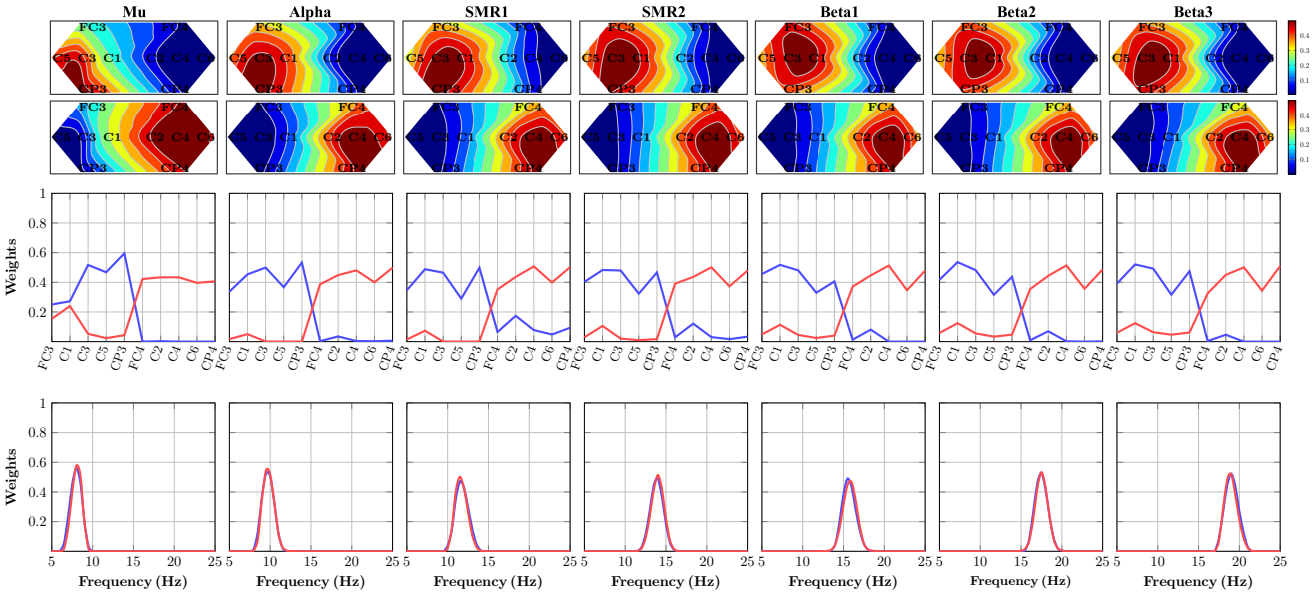

Figure 4: Subjet 1. The general PARAFAC spatial (*third row*) and frequency (*fourth row*) atoms obtained from multi-channel EEG recorded during MIEC. The weights were averaged over all available training days. The blue and red colors indicate the lateralized spatial distribution of the oscillatory EEG activities in the affected (left) and unaffected (right) hemispheres over the sensorimotor cortex. The scalp topography maps correspond to the general spatial atoms of the left (*first row*) and right (*second row*) hemispheres.

3.2 Oscillatory rhythms underlying MIEO

The result of PARAFAC decomposition during MIEO is presented in Figure 5. As expected, the PARAFAC model detected the same frequency signatures for MIEO as during the MIEC condition (see Figure 4). From Figure 5, as our expectation, we can see the PARAFAC model detected the same frequency signatures for movement imagery with open-eyes as the closed-eye condition. The only difference was found in the Beta 3 band, in which the central peak frequency was slightly different and located at 19 Hz. This shift can be because of the PARAFAC numerical issues.

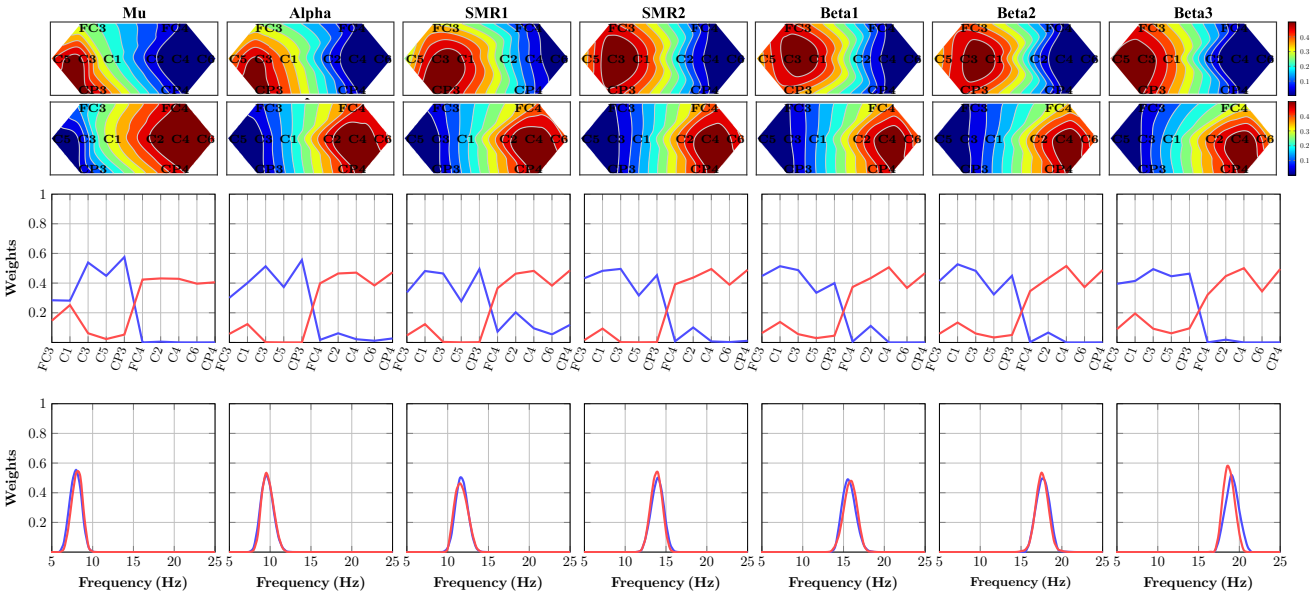

Figure 5: Subject 1. The general PARAFAC spatial (*third row*) and frequency (*fourth row*) atoms obtained from multi-channel EEG signal recorded during MIEO. The weights were averaged over all available training days. The blue and red colors indicate the lateralized spatial distribution of the oscillatory EEG activities in the affected (left) and unaffected (right) hemispheres over the sensorimotor cortex. The corresponding scalp topography maps of the identified spatial atoms over the left (*first row*) and right (*second row*) hemispheres are illustrated.

3.3 Between subjects stability of PARAFAC atoms

The PARAFAC model detected seven motor-related frequency signatures with highly stable peak frequencies among all subjects during rehabilitation training using MI BCI. This global stability is also clear over both affected (6; first row) and unaffected (7; first row) hemispheres. Furthermore, similarly to frequency signatures, spatial signatures represent the location of these motor-related oscillatory EEG sources either in the affected (6; second row) or unaffected (7; second row) hemisphere showing a high stability among all subjects.

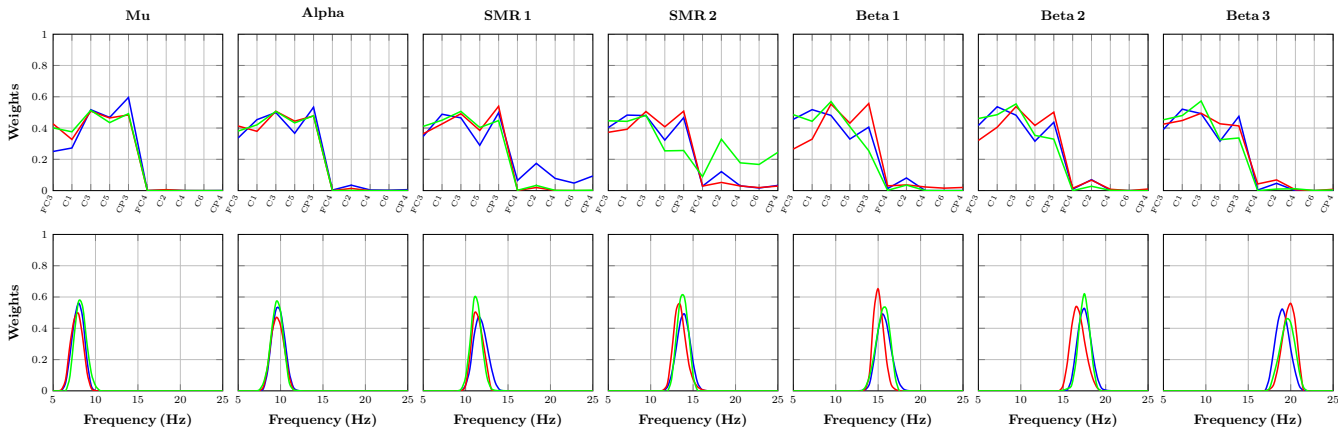

Figure 6: An example of highly stable general frequency (*top*) and spatial (*bottom*) PARAFAC atoms for Subject 1 (blue), Subject 2 (red), and Subject 3 (green) over the affected (left) cortex during MIEC.

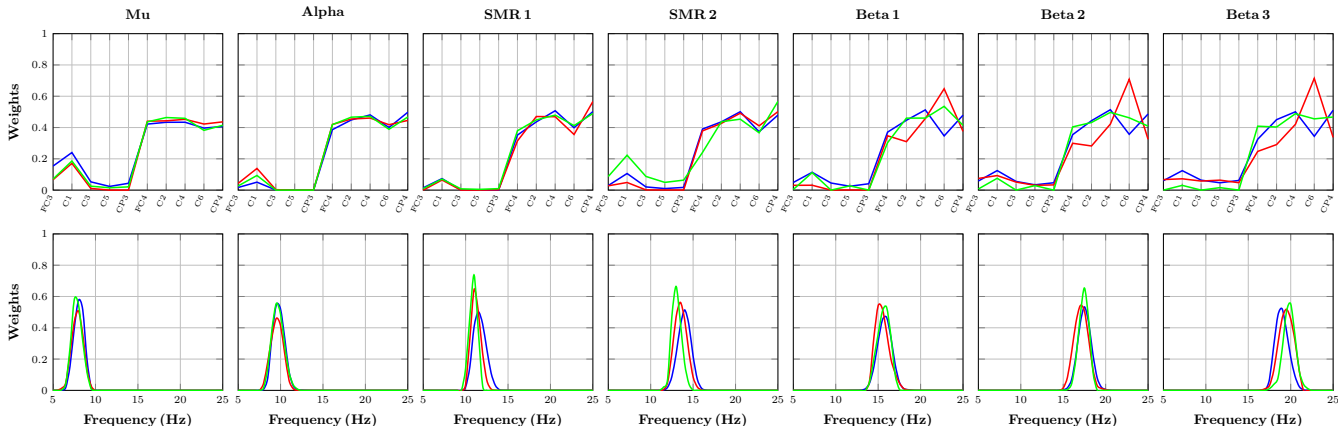

Figure 7: An example of highly stable general frequency (*top*) and spatial (*bottom*) PARAFAC atoms for Subject 1 (blue), Subject 2 (red), and Subject 3 (green) over the unaffected (right) cortex during MIEC.

3.4 Generating atom-specific PARAFAC time scores

For generating time scores, the PARAFAC weights of spatial and spectral atoms from all available training days and from each MIEC and MIEO conditions were firstly averaged together to obtain general atom weights. Then, for time score analysis reported in section 4, we projected the general atoms to the corresponding resting state (REC and REO) periodic EEG spectrum, estimated for two-second sliding windows with an overlap of 500 ms, of each training day. Similarly, for analysis reported in sections 5 and 6, the general spatial and spectral atoms were projected to the periodic EEG spectrum during MI estimated for two-seconds long overlapping segments with a sliding step size of 7.8125 ms (i.e. one data

point shift). In atom specific time scores, the spatial information obtained from all electrodes used in tensor construction and the spectral information of a given atom is embedded. It means that we have a discrete time score for a given frequency signature and each spatial lateralization (see Figure 8). In other words, the projection resulted in generating a numerical sequence called *time score* (TS), in which each value of the time score represents the presence of a specific atom (in the EEG spectrum) and space at a given time.

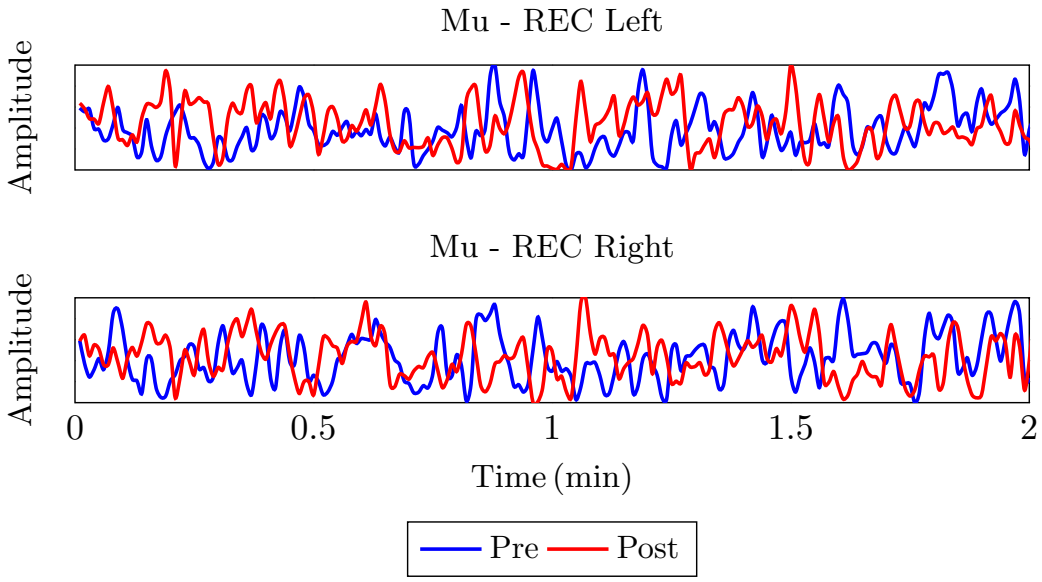

Figure 8: An example of Mu (8 Hz) PARAFAC time scores over the affected (*top*) and unaffected (*bottom*) hemispheres of Subject 1 in the pre- (blue) and post-training (red) during the REC condition. Each sample of time scores is a projection of general spatial and frequency weights obtained by the PARAFAC model onto a two-seconds artefact-free EEG epoch. The data were selected randomly from available training days and rescaled between 0 and 1 for better visualization.

4 Longitudinal analysis of neuroplastic changes in the sensorimotor rhythms following BCI rehabilitation

4.1 Longitudinal analysis of short-term MI BCI effects

In the REC condition, the Mu ($p < .001$), Alpha ($p = .004$), SMR 1 ($p < .001$), and SMR 2 ($p = .005$) PARAFAC average time scores of the affected (left) sensorimotor region increased significantly as a result of MI BCI training. Figures 9 (A) and 9 (C) present the day to day pre- and post-training changes obtained from time score analysis of Mu and SMR 1 over the affected cortex. By contrast, the mean PARAFAC time

scores in the different ranges of Beta, except Beta 3 ($p = .287$), showed significant post-training decreases (Beta 1; $p = .023$, Beta 2; $p < .001$). These results contrast with those obtained by the REO condition. The differences between pre- and post-training of PARAFAC time scores of the major identified frequency atoms were insignificant, except Mu and Alpha. For the REO condition, we observed a significant increase in Mu ($p = .001$) and Alpha ($p < .001$) time scores due to rehabilitation training, which is consistent with the results of the REC condition.

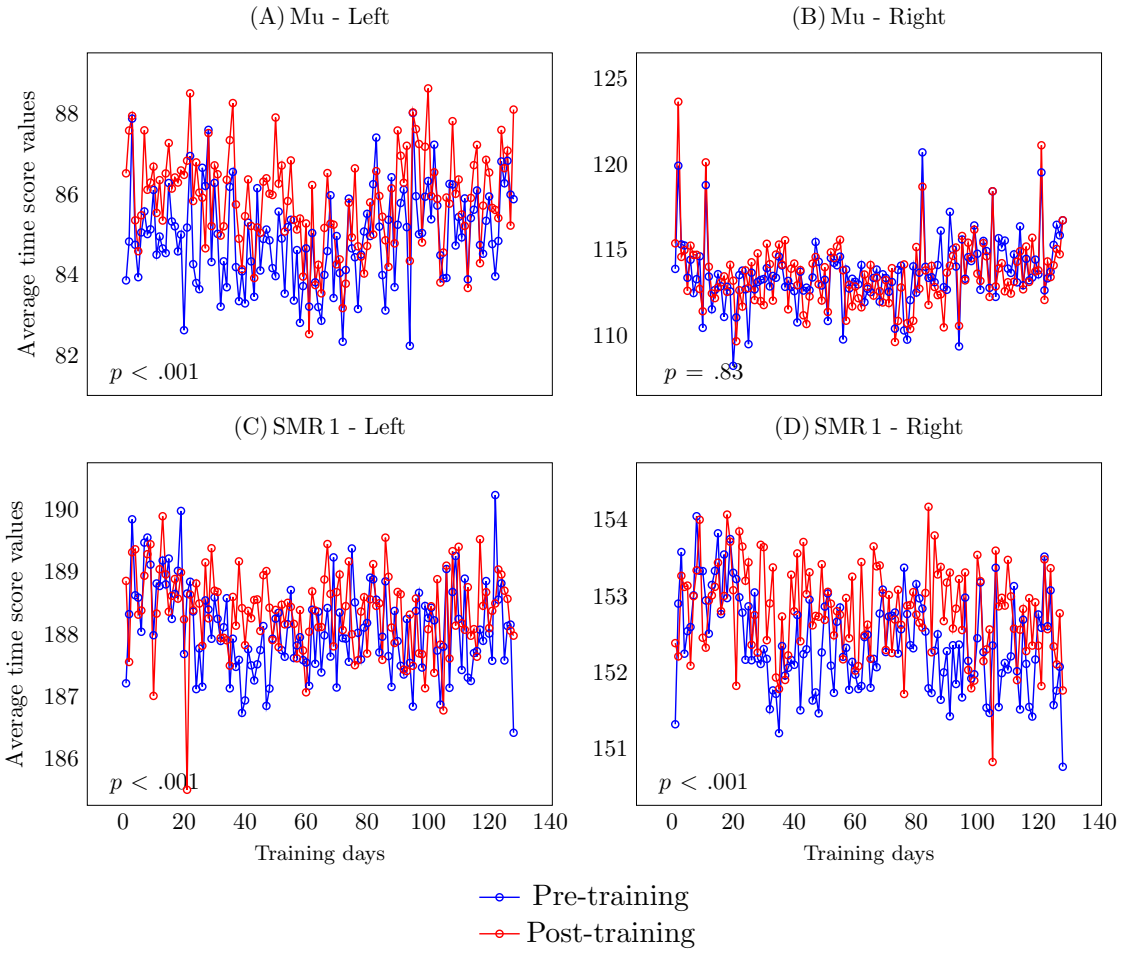

Figure 9: The mean values of Mu (*A, B*) and SMR 1 (*C, D*) PARAFAC time score changes over the affected (*left panel*) and unaffected (*right panel*) hemispheres between two resting periods, before (blue) and after (red) training during the REC condition. Each time score value represents an average computed for a training day using MI BCI coupled to a robotic device. The lateralized sensorimotor atoms were identified during the REC condition. Significant increases at the $p = 0.05$ level in Mu and SMR 1 time scores are indicated. Significant increases in Mu and SMR 1 time scores are indicated over the affected (*left panel*) and unaffected (*right panel*) hemispheres.

On the contrary to the left sensorimotor region, no significant post-training changes in the Mu, Alpha,

and Beta 1 PARAFAC time scores were found over the right hemisphere for the REC condition (all *p's* $> .174$). Similar to the affected hemisphere, post-training significant increases in SMR 1 ($p < .001$) and SMR 2 ($p < .001$) and decreases in Beta 2 ($p < .001$) and Beta 3 ($p < .001$) PARAFAC time scores were observed in the right hemisphere. Figures 9 (B) and 9 (D) show the day to day pre- and post-training changes obtained from time score analysis of Mu and SMR 1 over the unaffected cortex. For the REO condition, we detected no significant differences between the pre- and post-training PARAFAC average time scores in Mu, SMR 1, and Beta 2 (all *p's* $> .417$). While, Alpha ($p < .001$), SMR 2 ($p < .001$), and Beta 1 ($p < .001$) time score were significantly increased from pre- to post-training following the intervention.

4.2 Longitudinal analysis of long-term MI BCI effects

We found substantial increases in PARAFAC pre-training time scores of Mu ($p = .037$) and Beta 3 ($p = .041$) atoms during the period of intervention in the REC condition. By contrast, there was a significant reduction in SMR 1 pre-training time scores ($p = .029$). Figure 10 (A and C) shows the long-term Mu and SMR 1 time score (over the affected cortex) changes throughout the intervention period. The difference between mean time score values of the post- and pre-training blocks of Mu showed a significant decrease for the REC condition throughout the training days ($p = .011$). The there were no significant long-term trends for the post- and pre-training block differences of other major rhythms (all *p's* $> .23$). In the REO condition, except trend-level decreases in SMR 2 ($p = .059$) and Beta 3 ($p = .070$) atoms, no pre-training effect was observed for other atoms throughout the training days (all *p's* $> .27$). None of the post-training (all *p's* $> .11$) time scores of motor-related atoms was also statistically changed during the intervention period. However, the difference between the post- and pre-training time scores indicated significant and trend-level significant increases for Alpha ($p = .043$) and Beta 1 ($p = .063$), respectively.

In the REC condition, pre-training Mu ($p < .001$) and SMR 1 ($p < .001$) time scores within the right sensorimotor cortex showed remarkable long-term increasing and decreasing patterns over time, respectively. Moreover, except for SMR 1 ($p = .041$; Figure 10 B and D) and Beta 2 ($p = .030$) rhythms, none of the post-training time scores was statistically associated with the training period. Figure 10 (B and D) shows the long-term longitudinal Mu and SMR 1 time scores (over the unaffected cortex) changes during the training days. Furthermore, the post- and pre-training difference in REC time scores notably decreased in Mu ($p = .016$) and increased in SMR 2 ($p = .030$) atoms. while other motor-related time scores remained statistically stable throughout the training sessions (all *p's* $> .077$). The pre-training time scores were not associated with intervention time (all *p's* $> .08$) in the REO condition. In contrast, a strong increase in post-training time scores occurred for Mu ($p < .001$) rhythm. The longitudinal post-training time-scores changes remained insignificant for other atoms (all *p's* $> .079$). Marginally significant increases of the post- and pre-training difference associated with the rehabilitation period were only found in the SMR 2 ($p = .047$) and Beta 1 ($p = .057$) atoms, not in other atoms (all *p's* $> .10$).

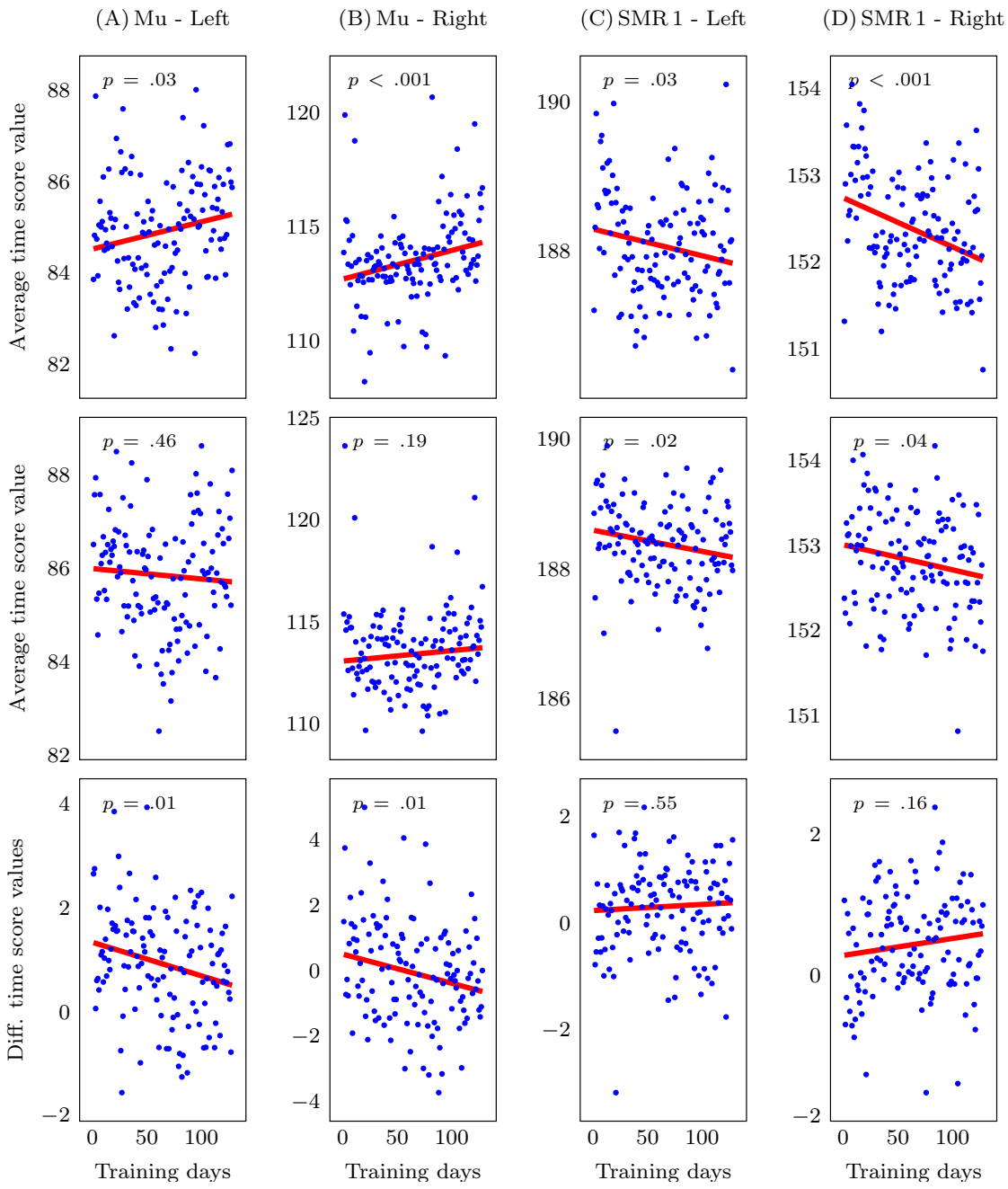

Figure 10: Association of longitudinal Mu (A&B) and SMR 1 (C&D) PARAFAC time scores changes in the pre-training block (*first row*), post-training block (*second row*), and the post- and pre-training differences (*third row*) with the intervention time. The sensorimotor atoms were identified during the REC condition over the affected (A&C) and unaffected (B&D) hemispheres. Each time score value represents an average computed for a training day using MI BCI coupled to a robotic device. The red lines represent a robust linear regression model fitted to data.

5 Dynamics of sensorimotor modulations underlying MI with eyes closed

5.1 Dynamic characteristics of MIEC during movement initiation

The PARAFAC time scores of each identified narrow-band EEG oscillatory rhythm was segmented into 7-second epochs, containing 2 sec before stimulus onset (*Move Command*) as a baseline to 5 sec after it (see Figure 1). Then, all trials obtained through all rehabilitation sessions for each patient were averaged to smooth the data and reduce the variability, leading to the enhancement of the signal-to-noise ratio. The possible similarities or dissimilarities of the time-locked temporal dynamics with the standard time-frequency analysis, known ERSP, were further explored using the raw EEG signals recorded over C3 and C4 electrodes corresponding to the contralateral and ipsilateral motor areas. The temporal dynamics of baseline-corrected time score changes in each identified narrow-band EEG oscillatory rhythms were calculated individually during MIEC. Baseline-correction means using data over a baseline period, i.e. before stimulus onset (Move Command), to correct data over a post-stimulus interval, i.e. after stimulus onset (Move Command). Here, we used the z-score method for baseline-corrected time score analysis [Grandchamp and Delorme, 2011].

For Subject 1 (Figure 11; top), the Mu and Beta 1 rhythms dynamics closely matched, especially on the right hemisphere ipsilateral to the imagined hand movements with a strong desynchronization started 1 sec after the MI. The dynamics of both ipsilateral and contralateral sensorimotor cortices presented a similar synchronization in SMR 1 rhythm reached their maximum after 2.5 seconds after the MI. Moreover, the dynamics of ipsilateral and contralateral sensorimotor cortices in SMR 2 and Beta 3 rhythms showed an inverse relation with respect to MI, so that, in SMR 2 (Beta 3) rhythm, a strong synchronization over the contralateral (ipsilateral) sensorimotor cortex was associated with a subtle desynchronization over the ipsilateral (contralateral) sensorimotor cortex. An ipsilateral Alpha synchronization was found 2 second after starting MI, which was absent in the contralateral cortex. Again, an ipsilateral Beta 2 desynchronization was also identified 1.5 second after starting MI, which was missing in the contralateral cortex.

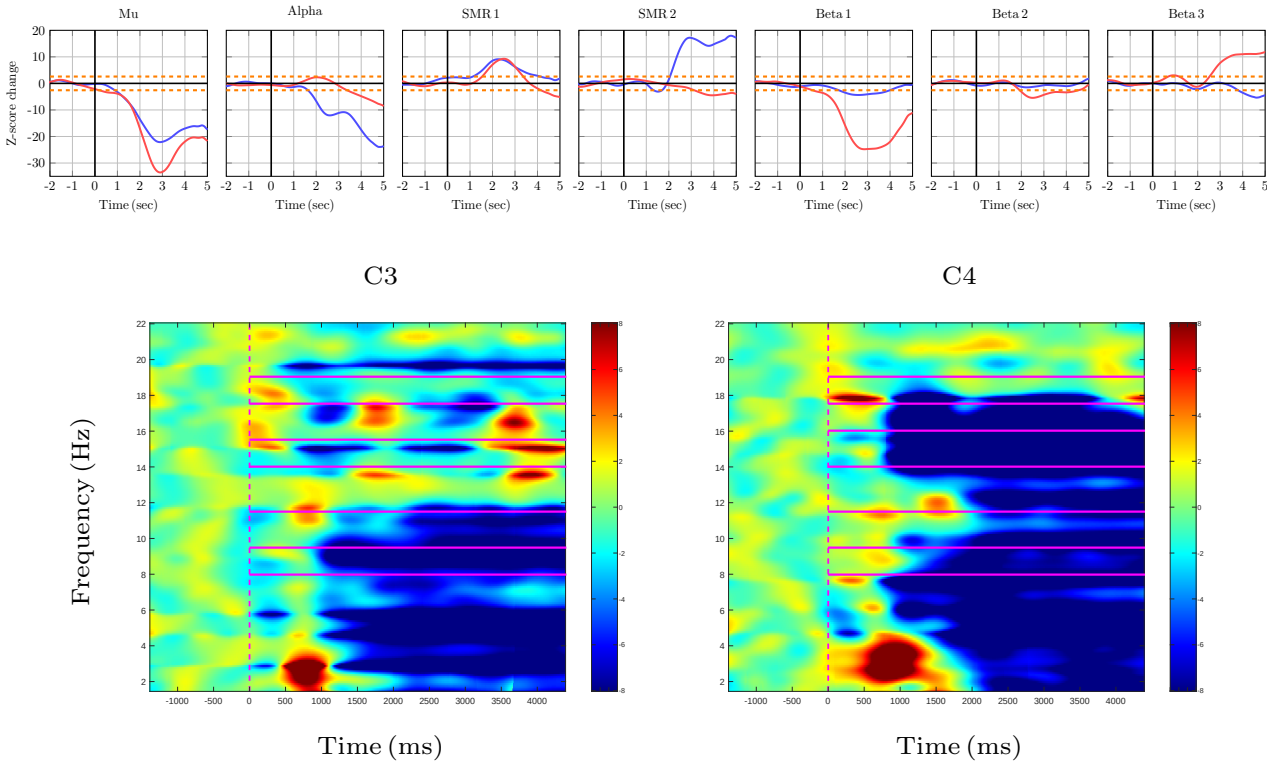

Figure 11: Subject 1. (*top*) Temporal dynamics of the baseline-corrected modulations of the identified narrow-band EEG rhythms during the MIEC in the affected (*blue*) and unaffected (*red*) sensorimotor cortices time-locked to the start of the motor imagery process. The dashed lines show the level of significance at 1%. (*bottom*) The corresponding ERSP plot to further validate the time score results were calculated for C3 (*left*) and C4 (*right*) EEG electrode sites. The pink lines indicate the subject-specific frequency peaks at 8.0 Hz (Mu), 9.5 Hz (Alpha), 11.5 Hz (SMR 1), 14.0 Hz (SMR 2), 15.5 Hz (Beta 1), 17.5 Hz (Beta 2), and 19.5 Hz (Beta 3) identified by tree-way PARAFAC model.

In summary, it can be concluded that Alpha, SMR 2, Beta 2, and Beta 3 rhythms over the ipsilateral cortex had different baseline-corrected temporal dynamic patterns compared to the contralateral cortex. The observed results are further supported by comparing the ERSP plot of C3 and C4 electrodes with those contralateral and ipsilateral time-locked temporal dynamics (Figure 11; bottom).

5.2 Dynamic characteristics of MIEC during movement completion

In this condition, the PARAFAC time scores of each identified narrow-band EEG oscillatory rhythm was segmented into 7-second epochs, containing 2 sec before stimulus onset (*Move Command*) as a baseline to 5 sec before hitting the robotic device. The temporal dynamics of contralateral sensorimotor cortex asso-

ciated with the affected area showed prominent desynchronizations only in the Mu and Alpha oscillatory rhythms, while the time-locked dynamics of the ipsilateral cortex presented significant desynchronizations in Mu and Beta 1 rhythms (see Figure 12, top). Furthermore, the desynchronization patterns mentioned above were closely matched with the corresponding ERSP plots (Figure 12, bottom) computed for C3 and C4 electrodes, representing the affected and unaffected cortices. The contralateral SMR 1 and SMR 2 synchronizations were also reflected in the ERSP at C3 electrode.

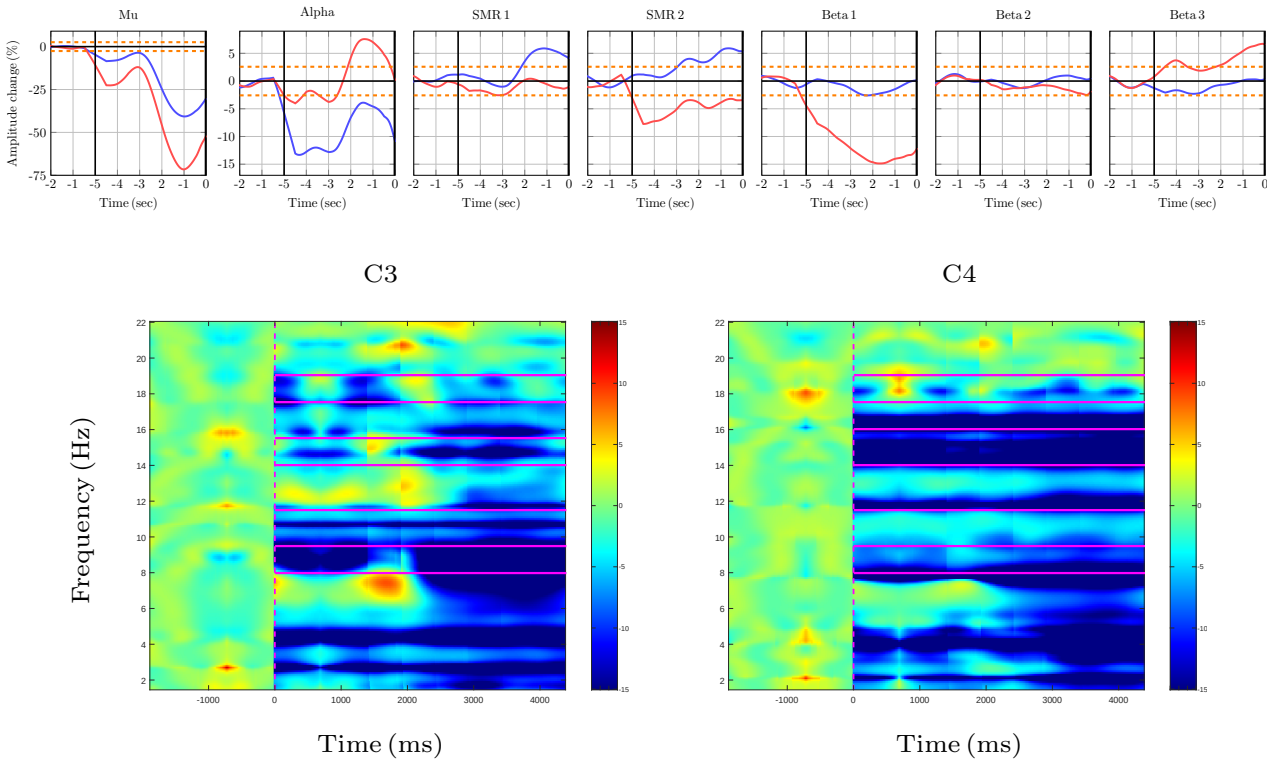

Figure 12: Subject 1. (*top*) The temporal dynamics of the baseline-corrected TS changes of the identified narrow-band EEG rhythms during MIEC in the affected (*blue*) and unaffected (*red*) sensorimotor cortices time-locked to the start of the MI process. The dashed lines shows the level of significance at 1%. (*bottom*) The corresponding ERSP plot to further validate the time score results were calculated for C3 (*left*) and C4 (*right*) EEG electrode sites. The pink lines indicate the subject-specific frequency peaks at 8.0 Hz (Mu), 9.5 Hz (Alpha), 11.5 Hz (SMR 1), 14.0 Hz (SMR 2), 15.5 Hz (Beta 1), 17.5 Hz (Beta 2), and 19.5 Hz (Beta 3) identified by tree-way PARAFAC model. Zero milliseconds in these ERSP plots correspond to five seconds before hitting the robotic device.

5.3 Consistency of MIEC dynamic characteristics

Figure 13 shows that the contralateral (top panels) and ipsilateral (bottom panels) Mu rhythms' oscillatory dynamics of all the subjects are consistent, suggesting the activities falling between 7.5 to 8.75 Hz (Mu rhythms) are a reliable signal for controlling the robotic device. A similar consistency in oscillatory dynamics of contralateral and ipsilateral 11.0 to 13.0 Hz (SMR 1 rhythms) was also observed. A closer look at the interplay between Mu (blue) and SMR 1 (red) rhythms is provided in Figure 13 revealing the differential contribution of these narrow-band oscillations with respect to the movement simulation. Furthermore, SMR 1 rhythm synchronization precedes Mu desynchronization, showing the potential of considering this rhythm (SMR 1) as an alternative control signal in BCI systems.

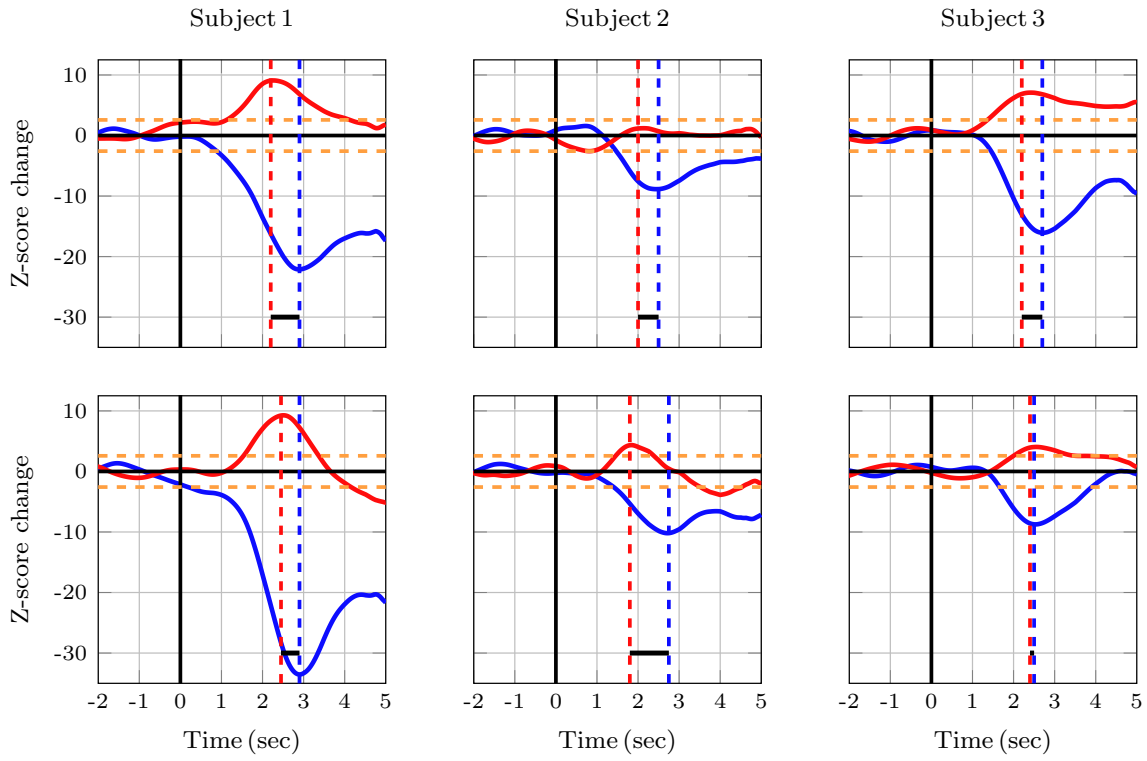

Figure 13: The temporal dynamics of the baseline-corrected Mu (*blue*) and SMR 1 (*red*) rhythms time-locked to the start of the MI process for Subject 1 (*first column*), Subject 2 (*second column*), and Subject 3 (*third column*). The temporal dynamics of the affected (*top*) and unaffected (*bottom*) cortices during MIEC condition are indicated by blue and red, receptively. The vertical dashed lines indicate the time when each rhythm reach to its maximum. The horizontal dashed lines show the level of significance at 1%.

6 Dynamics of sensorimotor modulation underlying eyes conditions

6.1 Dynamic characteristics of MIEC vs. MIEO during movement completion

To investigate time-locked temporal dynamics underlying MI process with EC and EO, atom-specific time scores were studied within 4 sec time frame windows before triggering the robotic arm, relative to a baseline interval selected 2 sec before the movement preparation onset (*Pause Index*). To smooth the data and gain maximal signal-to-noise ratio, the trials' time scores were then separately averaged over the ipsilateral (right) and contralateral (left) sensorimotor cortices. Accordingly, in this step, only successful trials in which the patient was *able* to hit the robotic splint were included in calculating time score averages. From Figure 14, we can see that, in most motor-related rhythms, the dynamics of the imagery process with EC before hitting the robotic splint closely matches the dynamics observed for the MIEO condition. The baseline-corrected (z-score) time scores of MIEC prominently decreased in Alpha (10 Hz atom) but increased in SMR 1 (11.5 Hz atom) and SMR 2 (14 Hz atom) oscillatory rhythms over the sensorimotor cortex contralateral to the hand used for imagery, as compared with MIEO. Furthermore, compared to the MI with open eyes, the magnitude of suppression in ipsilateral and contralateral Mu and ipsilateral Beta 1 (15.5 Hz atom) oscillatory rhythms over the sensorimotor network was strongest for imagined movement with closed eyes, as compared with MIEO.

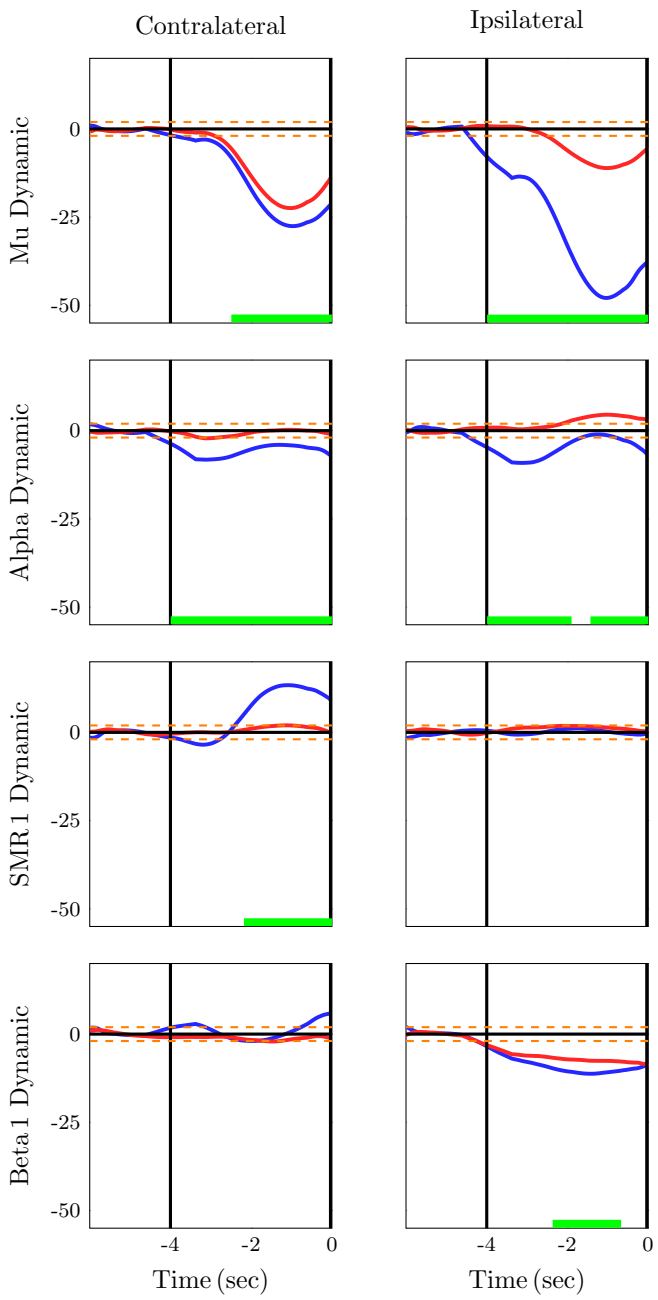

Figure 14: Temporal dynamics of the baseline-corrected Mu (*first row*), Alpha (*second row*), SMR 1 (*third row*), Beta 1 (*forth row*) oscillatory atom modulations during movement execution. The time scores were detected over the sensorimotor cortex contralateral (*left column*) and ipsilateral (*right column*) to the imagined hand during MIEC (blue) and MIEO (red) conditions. The dashed lines show the level of significance at 5%.

6.2 Dynamic characteristics of MIEC vs. MIEO during movement preparation and movement initiation

Tor this purpose, the ipsi- and contralateral time scores of each identified frequency atom representing narrow-band EEG oscillatory rhythms was segmented into 14-second epochs. In other words, each epoch included a time frame of 2 sec before the movement preparation onset (*Pause Index*) considered as a baseline, 6 sec movement preparation phase (between the *Pause Index* and the *Move Command* presentation), and 6 s after the sound cue presentation (i.e. MI onset) considered as movement initiation phase (Figure 15). In the movement preparation phase, there were strong enhancements in Beta 1 time scores over both ipsi- and contralateral sensorimotor cortices for MIEC compared to MIEO. In contrast, the baseline-corrected time score of Alpha rhythm ipsilateral to the hand used for imagery showed a significant decrease for MIEC compared with the MIEO during the movement preparation phase. When the patient started to imagine the movement of his affected with closed eyes, the magnitude time score suppression of Mu and Alpha rhythms over both ipsil- and contralateral sensorimotor cortices, and Beta 1 rhythm over the ipsilateral cortex were significantly higher compared with the MIEO trials.

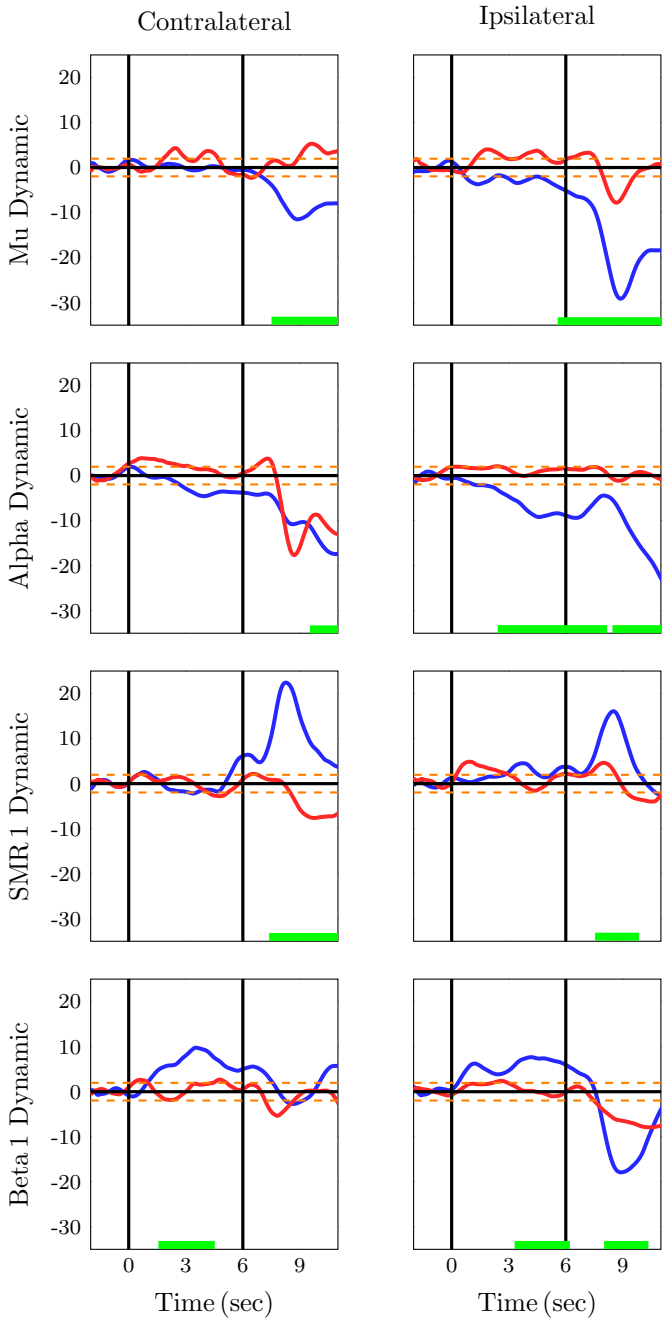

Figure 15: Temporal dynamics of the baseline-corrected Mu (*first row*), Alpha (*second row*), SMR 1 (*third row*), Beta 1 (*forth row*) oscillatory atom modulations during movement preparation and movement imagery. The time scores were detected over the sensorimotor cortex contralateral (*left column*) and ipsilateral (*right column*) to the imagined hand during MIEC (blue) and MIEO (red) conditions. The dashed lines show the level of significance at 5%.

7 Conclusion and contributions of the thesis

EEG based BCI-assisted rehabilitative technologies show promising clinical results in the functional recovery of stroke patients. However, a better understanding of the BCI effects on the sensorimotor repair mechanisms is still needed. In this thesis, to identify the main profiles of high-dimensional EEG data and simplify the data structure by reducing the dimensionality, we employed an advanced analytical framework based on tensor decomposition. In particular, in this thesis, we expanded on the work of Rosipal et al. [2019], who suggested and developed a tensor-based paradigm to study the neural modulations underpinning longitudinal mirror-box therapy.

There were two primary aims of this study: (I) To contribute to a deeper understanding of longitudinal neuroplastic changes in the sensorimotor rhythms following a course of motor rehabilitation using robotic-assisted MI BCI. (II) To expound on the sensorimotor modulation dynamics during different phases of MI while patients performed the imagery task with their eyes both open and closed. In this thesis we have attempted to address the questions mentioned above by exploring the potential benefits of tensor decomposition methods in measuring cortical motor-related neural sources of the brain. The main results and contributions of the thesis are as follow:

- One of the major parts of the thesis was to precisely identify dominant subject-specific motor-related cortical rhythms by an analytical tensor decomposition framework. Using this approach, we detected a set of highly stable narrow-band oscillatory rhythms, consistently observed among the post-stroke subjects. The results were approximately the same regardless of whether the eyes were open or closed or the PARAFAC or Tucker models were used. The achieved results were published in Rošťáková et al. [2020b] and presented at Rošťáková et al. [2020a].

- Based on our quantitative analysis results, we showed that longitudinal motor training of stroke patients using robotic-assisted MI BCI might induce neuroplastic alterations in the motor cortex, which are associated with long-lasting changes in the brain's electrical activity. Importantly, we observed that narrow-band slow (in the range of ~ 7.5 Hz to ~ 8.75 Hz) and fast EEG sensorimotor rhythms played longitudinally distinct but complementary roles in the recovery of motor functions.

- During motor imagery of the affected hand with eyes closed (MIEC), we found a functional dissociation of subject-specific Mu (~ 8 Hz) and SMR 1 (~ 11.5 Hz) oscillatory rhythms, in which SMR 1 synchronization preceded Mu desynchronization. This shows the potential of considering SMR 1 (especially those belonging to the ipsilateral side) as a supplementary control signal in BCI systems.

- We found that the oscillatory neural activity during eyes-closed (MIEC) and eyes-open (MIEO) motor imagery were modulated differently, providing additional evidence that closed-eyes and open-eyes are fundamentally different behaviors [Marx et al., 2004; Rimbert et al., 2018]. We investigated the potential differences of the MIEC and MIEO dynamics in the various time frames of the MI task,

including movement preparation, movement initiation, and movement completion phases. When MIEC trials were compared to MIEO, three key narrow-band rhythms were identified with differently modulated oscillatory dynamics:

1. Beta 1 (~ 15.5 Hz, ipsi- and contralateral) in the movement preparation phase
2. Contralateral Mu and SMR 1 in the movement initiation phase
3. Contralateral SMR 1 in the movement completion phase

- We found that tensor decomposition of EEG signals broadens our understanding of the neural mechanism underlying human motor-related behavior. For future BCI-EEG research, our observations call for narrow-band-oriented analysis in place of canonical wide-range frequency bands, which contain a number of oscillatory rhythms with varying modulatory effects.

The results of the current study manifest the application potential of the tensor-based analysis in quantitative evaluation of cortical modulations in the sensorimotor EEG rhythms of post-stroke patients measured during longitudinal robotic-assisted MI BCI training. Clearly, strict clinical observations are required to assess the efficacy of treatment strategies and narrow-band distinct sensorimotor modulations. Finally, we can conclude that the tensor-based analysis applied to measured BCI-EEG data throughout this thesis may provide an effective alternative analytical framework to the current univariate approaches in BCI research, offering an in-depth insight into the human sensorimotor system.

References

Ang, K. K., Guan, C., Chua, K. S. G., Ang, B. T., Kuah, C. W. K., Wang, C., Phua, K. S., Chin, Z. Y., and Zhang, H. (2011). A large clinical study on the ability of stroke patients to use an EEG-based motor imagery brain-computer interface. *Clinical EEG and Neuroscience*, 42(4):253–258. doi:10.1177/155005941104200411.

Bro, R. et al. (1997). PARAFAC. Tutorial and applications. *Chemometrics and intelligent laboratory systems*, 38(2):149–172. doi:10.1016/S0169-7439(97)00032-4.

Buch, E., Weber, C., Cohen, L. G., Braun, C., Dimyan, M. A., Ard, T., Mellinger, J., Caria, A., Soekadar, S., Fourkas, A., et al. (2008). Think to move: a neuromagnetic brain-computer interface (BCI) system for chronic stroke. *Stroke*, 39(3):910–917. doi:10.1161/STROKEAHA.107.505313.

Chaudhary, U., Birbaumer, N., and Ramos-Murguialday, A. (2016). Brain–computer interfaces for communication and rehabilitation. *Nature Reviews Neurology*, 12(9):513–525. doi:10.1038/nrneurol.2016.113.

Cichocki, A., Mandic, D., De Lathauwer, L., Zhou, G., Zhao, Q., Caiafa, C., and Phan, H. A. (2015). Tensor decompositions for signal processing applications: From two-way to multiway component analysis. *IEEE signal processing magazine*, 32(2):145–163. doi:10.1109/MSP.2013.2297439.

Cichocki, A., Washizawa, Y., Rutkowski, T., Bakardjian, H., Phan, A.-H., Choi, S., Lee, H., Zhao, Q., Zhang, L., and Li, Y. (2008). Noninvasive BCIs: Multiway signal-processing array decompositions. *Computer*, 41(10):34–42. doi:10.1109/MC.2008.431.

Cong, F., Lin, Q.-H., Kuang, L.-D., Gong, X.-F., Astikainen, P., and Ristaniemi, T. (2015). Tensor decomposition of EEG signals: A brief review. *Journal of neuroscience methods*, 248:59–69. doi:10.1016/j.jneumeth.2015.03.018.

Delorme, A. and Makeig, S. (2004). EEGLAB: an open source toolbox for analysis of single-trial EEG dynamics including independent component analysis. *Journal of neuroscience methods*, 134(1):9–21. doi:10.1016/j.jneumeth.2003.10.009.

Donoghue, T., Schaworonkow, N., and Voytek, B. (2021). Methodological considerations for studying neural oscillations. *European Journal of Neuroscience*. doi:10.1111/ejn.15361.

Grandchamp, R. and Delorme, A. (2011). Single-trial normalization for event-related spectral decomposition reduces sensitivity to noisy trials. *Frontiers in psychology*, 2:236. doi:10.3389/fpsyg.2011.00236.

Harshman, R. A. (1970). Foundations of the PARAFAC procedure: Models and conditions for an "explanatory" multimodal factor analysis. *UCLA Working Papers in Phonetics*, 16:1–84.

Kapreli, E., Athanasopoulos, S., Papathanasiou, M., Van Hecke, P., Strimpakos, N., Gouliamos, A., Peeters, R., and Sunaert, S. (2006). Lateralization of brain activity during lower limb joints movement. An fMRI study. *Neuroimage*, 32(4):1709–1721. doi:10.1016/j.neuroimage.2006.05.043.

Liu, Y., Li, M., Zhang, H., Wang, H., Li, J., Jia, J., Wu, Y., and Zhang, L. (2014). A tensor-based scheme for stroke patients' motor imagery EEG analysis in BCI-FES rehabilitation training. *Journal of neuroscience methods*, 222:238–249. doi:10.1146/annurev.psych.48.1.269.

Marx, E., Deutschländer, A., Stephan, T., Dieterich, M., Wiesmann, M., and Brandt, T. (2004). Eyes open and eyes closed as rest conditions: impact on brain activation patterns. *Neuroimage*, 21(4):1818–1824. doi:10.1016/j.neuroimage.2003.12.026.

Monge-Pereira, E., Ibañez-Pereda, J., Alguacil-Diego, I. M., Serrano, J. I., Spottorno-Rubio, M. P., and Molina-Rueda, F. (2017). Use of electroencephalography brain-computer interface systems as a rehabilitative approach for upper limb function after a stroke: a systematic review. *PM&R*, 9(9):918–932. doi:10.1016/j.pmrj.2017.04.016.

Murphy, T. H. and Corbett, D. (2009). Plasticity during stroke recovery: from synapse to behaviour. *Nature Reviews Neuroscience*, 10(12):861–872. doi:10.1038/nrn2735.

Nunez, P. L., Srinivasan, R., et al. (2006). *Electric fields of the brain: the neurophysics of EEG*. Oxford University Press, USA.

Rimbert, S., Al-Chwa, R., Zaepffel, M., and Bougrain, L. (2018). Electroencephalographic modulations during an open-or closed-eyes motor task. *PeerJ*, 6:e4492. doi:10.7717/peerj.4492.

Rosipal, R., Porubcová, N., Barančok, P., Cimrová, B., Farkaš, I., and Trejo, L. J. (2019). Effects of mirror-box therapy on modulation of sensorimotor EEG oscillatory rhythms: a single-case longitudinal study. *Journal of neurophysiology*, 121(2):620–633. doi:10.1152/jn.00599.2018.

Rosipal, R., Rošt'áková, Z., and Trejo, L. J. (2022). Tensor Decomposition of Human Narrow-band Oscillatory Brain Activity in Frequency, Space and Time. *Biological Psychology*, page 108287. doi:10.1016/j.biopsycho.2022.108287.

Rošťáková, Z., Rosipal, R., and Seifpour, S. (2020a). Tucker Tensor Decomposition of Multi-session EEG Data. In *International Conference on Artificial Neural Networks*, pages 115–126. Springer. doi:10.1007/978-3-030-61609-0-10.

Rošťáková, Z., Rosipal, R., Seifpour, S., and Trejo, L. J. (2020b). A Comparison of Non-negative Tucker Decomposition and Parallel Factor Analysis for Identification and Measurement of Human EEG Rhythms. *Measurement Science Review*, 20(3):126–138. doi:10.2478/msr-2020-0015.

Seeck, M., Koessler, L., Bast, T., Leijten, F., Michel, C., Baumgartner, C., He, B., and Beniczky, S. (2017). The standardized EEG electrode array of the IFCN. *Clinical Neurophysiology*, 128(10):2070–2077. doi:10.1016/j.clinph.2017.06.254.

Tangwiriyasakul, C., Premoli, I., Spyrou, L., Chin, R. F., Escudero, J., and Richardson, M. P. (2019). Tensor decomposition of TMS-induced EEG oscillations reveals data-driven profiles of antiepileptic drug effects. *Scientific reports*, 9(1):1–11. doi:10.1038/s41598-019-53565-9.

Toga, A. W. and Thompson, P. M. (2003). Mapping brain asymmetry. *Nature Reviews Neuroscience*, 4(1):37–48. doi:10.1038/nrn1009.

Tucker, L. R. (1966). Some mathematical notes on three-mode factor analysis. *Psychometrika*, 31(3):279–311. doi:10.1007/BF02289464.

Watrous, A. J. and Buchanan, R. J. (2020). The Oscillatory ReConstruction Algorithm adaptively identifies frequency bands to improve spectral decomposition in human and rodent neural recordings. *Journal of Neurophysiology*, 124(6):1914–1922. doi:10.1152/jn.00292.2020.

Wen, H. and Liu, Z. (2016). Separating fractal and oscillatory components in the power spectrum of neurophysiological signal. *Brain topography*, 29(1):13–26. doi:10.1007/s10548-015-0448-0.

List of author's publications

- Rošťáková Z, Rosipal R, **Seifpour S**, Trejo LJ. A comparison of nonnegative Tucker decomposition and parallel factor analysis for identification and measurement of human EEG rhythms. *Measurement Science Review*, Volume 20, pp. 126-138, **2020**, DOI: 10.2478/msr-2020-0015, **Cited 4 times** in:

  (I) Zdunek, R; Fonal, K, Volume 14, Issue 1, Article Number 113, DOI 10.3390/sym14010113, Published JAN 2022.
  (II) Bhatt, V; Kumar, S; Saini, S, Volume 46, Page 10787-10792, DOI 10.1016/j.matpr.2021.01.676, Published 2021.
  (III) Yang, L; Chen, HX; Ke, Y; Li, ML; Huang, L; Miao, YZ, Volume 2021, Issue 1, Article Number 37, DOI 10.1186/s13634-021-00730-w, Published JUL 13 2021.
  (IV) Li, K; Wang, J; Li, SS; Yu, HT; Zhu, L; Liu, J; Wu, LY, Volume 29, Page 1557-1567, DO I10.1109/TNSRE.2021.3101240, Published 2021.

- Rošťáková Z, Rosipal R, **Seifpour S**. Tucker tensor decomposition of multi-session EEG data. In ICANN 2020: *Lecture Notes in Computer Science : Artificial Neural Networks and Machine Learning*, vol. 12396, pp. 115-126, **2020**, DOI: 10.1007/978-3-030-61609-0_10.

Publication under review:

- **Seifpour S**, Rošťáková Z, Šatka A. A tensor-based analysis of longitudinal neuroplastic changes in the sensorimotor brain rhythms following BCI stroke rehabilitation. *Under review in the Journal of IEEE Transactions on Neural Systems and Rehabilitation Engineering.*

List of other author's publications (selected)

- **Seifpour S**, Niknazar H, Mikaeili M, Nasrabadi A. M. A new automatic sleep staging system based on statistical behavior of local extrema using single-channel EEG signal. *Expert Systems with Applications*, Volume 104, pp. 277-293, **2018**, DOI: 10.1016/j.eswa.2018.03.020 (**Cited 26 times**).

- Saghayan MH, **Seifpour S**, Khadem A. Automated sleep stage scoring using brain effective connectivity and EEG signals. In ICSPIS 2021: 7^{th} *International Conference on Signal Processing and Intelligent Systems*, pp. 1-5, **2021**, DOI: 10.1109/ICSPIS54653.2021.9729377.

- Nouri A, Esmaeili F, **Seifpour S**, Talkhabi M, Khorrami A. The impact of dialogic learning on students' attention and academic achievements. *Annals of Behavioral Neuroscience*, Volume 1, pp. 47-55, **2018**, DOI: 10.18314/abne.v1i1.1215.

- Bayatfar S, **Seifpour S**, Asghari-Oskoei M, Khadem A. An automated system for diagnosis of sleep apnea syndrome using single-channel EEG signal. In ICEE 2019: *27th Iranian Conference on Electrical Engineering*, pp. 1829-1833, **2019**, DOI: 10.1109/IranianCEE.2019.8786667.

- Niknazar H, **Seifpour S**, Mikaeili M, Nasrabadi A. M, Khorrami A. A novel method to detect the A phases of cyclic alternating pattern (CAP) using similarity index. In ICEE: *23rd Iranian Conference on Electrical Engineering*, pp. 67-71, **2015**, DOI: 10.1109/IranianCEE.2015.7146184 (**Cited 6 times**).

- **Seifpour S**, Sadeghniiat K, Mikaeili M, Khorrami A, Nami M, Alemohammad Z. B. Investigating the role of sleep in emotional memory processing; A pilot study based on analysis of inverse efficiency score. *7th World Congress on Sleep Medicine*, volume 40, p. e9, ISSN 1389-9457, **2017**, DOI: 10.1016/j.sleep.2017.11.020.

- **Seifpour S**, Khorrami A, Nami M, Sadeghniiat K, Mikaeili M, Hekmatmanesh A. Learning of emotional and non-emotional visual stimuli is related to sleep macrostructure. *6th World Congress on Sleep Medicine*, volume 16, p. S250, ISSN 1389-9457, **2015**, DOI: 10.1016/j.sleep.2015.02.1540.

- **Seifpour S**, Mikaeili M, Sadeghniiat K, Hekmatmanesh A, Khorrami A. Expose to emotional stimuli change the microstructural sleep electroencephalography. In Journal of Sleep Research: *22ndCongress of the European Sleep Research Society*, volume 23, p. 604, **2014**.

- Hekmatmanesh A, Mikaeili M, Sadeghniiat K, **Seifpour S**, Khorrami A. Spindles affection by use of negative emotional stimulations. In Journal of Sleep Research: *22ndCongress of the European Sleep Research Society*, volume 23, p. 99, **2014**.